Magnetic structure of the double perovskite La$_2$NiIrO$_6$ investigated using neutron diffraction

Shivani Sharma [1,2,*] C. Ritter [3,†] D. T. Adroja [1,4,‡] G. B. Stenning,[1] A. Sundaresan,[2] and S. Langridge[1]

[1]*ISIS facility, Rutherford Appleton Laboratory, Chilton Oxon, OX11 0QX, United Kingdom*

[2]*Jawaharlal Nehru Centre for Advanced Scientific Research, Jakkur, Bangalore 560064, India*

[3]*Institut Laue-Langevin, 71 Avenue des Martyrs, CS 20156, 38042, Grenoble Cedex 9, France*

[4]*Highly Correlated Matter Research Group, Physics Department, University of Johannesburg, Auckland Park 2006, South Africa*

A polycrystalline sample of La$_2$NiIrO$_6$ has been synthesized and characterized using magnetization and neutron powder diffraction to explore the magnetic ground state. Three anomalies are evident in the bulk magnetization measurements at 28, 50, and 74 K, of which only the 74 K transition is associated with long-range ordering of Ni^{2+} and Ir^{4+} spins. The neutron thermodiffractogram recorded between 1.5 and 90 K and Rietveld refinements of the temperature difference data 1.5–90 K, 40–90 K, and 62–90 K confirm that both the Ni and Ir moments order at the same temperature below 74 K. No change in the magnetic peak intensities or new peaks have been found further below 50 and 28 K indicating that the spin structure remains the same down to 1.5 K. The magnetic propagation vector is $k = (\frac{1}{2}, \frac{1}{2}, 0)$ and the estimated magnetic moment values at 1.5 K are $\mu_{\mathrm{Ni}} = 1.39(8)\mu_{\mathrm{B}}$ and $\mu_{\mathrm{Ir}} = 0.35(3)\mu_{\mathrm{B}}$. Contrary to a recent publication by Ferreira *et al.* [Phys. Rev. Mater. **5**, 064406 (2021)] on the same compound, the improved data quality allows now to ascertain the presence of an ordered moment on the iridium sites. The magnetic structure proposed by Ferreira *et al.* is discussed and it is shown that there are several magnetic structures compatible with the data but indistinguishable by neutron powder diffraction methods.

I. INTRODUCTION

Strongly correlated transition-metal oxides (TMOs) with partially filled *d* orbitals have been the subject of extensive investigations following the discovery of a variety of novel physical phenomena and a diversity of new phases [1–5]. Among these TMOs compounds, iridium (Ir)-based materials have very recently attracted considerable attention as the Ir ion can adopt different valence states, i.e., Ir^{4+} (5d^5, $S = 1/2$), Ir^{5+} (5d^4, $S = 1$), and Ir^{6+} (5d^3, $S = 3/2$) and thereby provides a tuning parameter for their physical properties. Ir compounds often possess comparable energy scales for the strong spin-orbit coupling (SOC), the on-site Coulomb repulsion (U), the crystal-field energy, the Hund coupling (J_{H}), the intersite hopping (t_{hop}), and the electronic bandwidth (W) which altogether affect in a variety of ways the ground state in these systems. Due to the fascinating physics and the possibility of tuning the ground state, iridates are interesting materials to study the various novel phases which originate from the spin-orbit entanglement combined with the crystal field. Iridium compounds with Ir^{4+} in IrO$_6$ octahedral environment host for example various captivating phenomena as revealed by experimental and theoretical results, such as Kitaev quantum spin liquid behavior in Li$_2$IrO$_3$ and Na$_2$IrO$_3$ [6], the quantum spin

Hall effect in Na$_2$IrO$_3$ [7], topological Mott insulator behavior in Ir pyrochlores [8,9], the Weyl semimetal state coexisting with noncollinear magnetic order in Y$_2$Ir$_2$O$_7$ [10], $J_{\mathrm{eff}} = 1/2$ Mott insulators [11–13], axion insulators [10,14], a half-metallic ferromagnet with the highest T_{C} in Sr$_2$CrIrO$_6$ [15], and theoretically predicted superconductivity in Sr$_2$IrO$_4$ [16].

One such class of materials which sees a significant role of Ir in determining the magnetic and transport properties is formed by iridium-based double perovskites with the general formula A$_2$BB$'$O$_6$ with $A =$ Ca, Ba, Sr, rare earth; $B =$ magnetic 3d/4d ions and nonmagnetic ions, such as Zn, Mg, In; and $B' =$ Ir [17–22]. The ability of Ir to display different oxidation states, through doping and substitution at the A and B sites of the double-perovskite structure has resulted in a rich variety of properties [23]. Although Ir^{4+} is the most common oxidation state, Ir^{+3} has been found at the octahedral site of double perovskites such as Sr$_2$TaIrO$_6$ and Sr$_2$NbIrO$_6$ [24]. A wide range of magnetic ground states observed in the double perovskites range from antiferromagnetic (AFM) to ferri- and ferromagnetic or short-range ordered spin-glass states [25–28].

The Ir-based double perovskites having a 3d metal at the B site have drawn special attention due to their interesting properties originating from the interplay of the 3d ion having strong electron correlation with the Ir ion where SOC plays a major role in deciding the physical and chemical properties [29–36]. In Ir-based double perovskites having IrO$_6$ octahedra, the Ir 5d levels split into e_g and t_{2g} levels under the octahedral crystal electric field (CEF). Due to the strong SOC,

———————
*phy.shivanisharma@gmail.com
†ritter@ill.fr
‡Devashibhai.adroja@stfc.ac.uk

the t_{2g} levels further split into a quartet ($J_{eff} = 3/2$) and a doublet ($J_{eff} = 1/2$) which plays a major role in deciding the magnetic ground state and most of the transport and magnetic properties in these oxides. In double perovskites having Ir ions in the Ir^{+4} oxidation state, the $5d^5$ electrons fill the low-lying quartet ($J_{eff} = 3/2$) and half of the doublet ($J_{eff} = 1/2$) states leading to a $J_{eff} = 1/2$ Mott spin-orbit insulating state. This leads to the interesting physical properties and magnetic ground states with a reduced moment of Ir in these systems [37]. The experimental observation by neutron diffraction of the ordered low-spin Ir moment is notoriously difficult due to its reduced moment value and due to the relatively strong neutron absorption of iridium. Nonetheless, high-intensity neutron powder diffraction (NPD) has recently been shown to detect the small Ir^{4+} moments as found in, e.g., the pyrochlore Nd$_2$Ir$_2$O$_7$ [38].

In the present work, we report x-ray diffraction (XRD), bulk magnetization, and detailed NPD results on La$_2$NiIrO$_6$ to elucidate the magnetic ground state. Based on the Rietveld refinement of high-intensity neutron powder diffraction data, La$_2$NiIrO$_6$ is found to undergo an AFM transition below 74 K with additional anomalies at low temperatures visible in the magnetization data, consistent with the literature [39]. The Rietveld refinement of the data reveals various possible magnetic ground states in La$_2$NiIrO$_6$, which are indistinguishable by NPD. Recently, Ferreira *et al.* [36], have presented a spin configuration for La$_2$NiIrO$_6$ which, as shown by this work, represents only one of the possible solutions. The presence of an ordered iridium ordering at the same temperature as the Ni moment can now be ascertained.

II. EXPERIMENT

A polycrystalline sample of La$_2$NiIrO$_6$ has been prepared via a solid-state reaction route [29]. The starting materials La$_2$O$_3$, NiO, and IrO$_2$ are mixed and grinded in stoichiometric ratio. The powder sample was calcined at 900 °C for 24 h and 1100 °C for 48 h. The powder was pressed into 10-mm pellets and the pellets were annealed at 1200 °C for 24 h. The annealed pellets were then crushed into a fine powder to check the phase purity via a Rigaku x-ray diffractometer equipped with a Cu-Kα source. The DC and AC magnetization have been measured as a function of temperature and magnetic field using a superconducting quantum interference device–vibrating-sample magnetometer. NPD measurements have been performed on the powdered samples using the high-intensity powder diffractometer D20 and the high-resolution powder diffractometer D2B, both situated at the Institut Laue-Langevin, Grenoble, France. Data were taken at 1.5 K and room temperature on D2B while temperature-dependent data were taken between 1.5 and 90 K on D20 using a ramp speed of 0.1 K every 48 s. Data were recorded for 10 min giving a temperature resolution of 1.25 K between adjacent datasets. Long measurements of 3 h each were taken at 1.5, 40, 62, and 90 K. Rietveld refinement of the powder XRD and NPD data have been performed using the FULL-PROF suite of programs [40]. Symmetry analysis was done using the program MAXMAGN of the Bilbao Crystallographic Server [41].
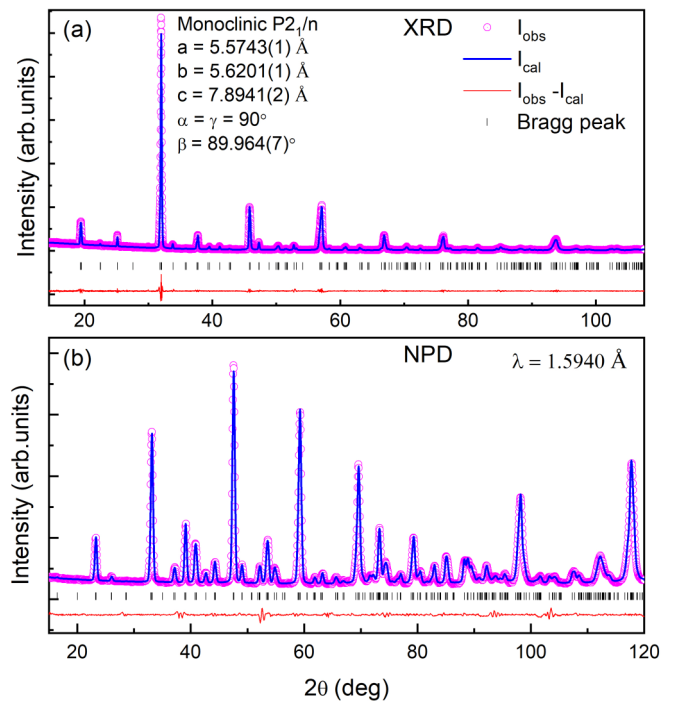

FIG. 1. Rietveld refined room-temperature (a) x-ray diffraction and (b) neutron powder diffraction patterns of La$_2$NiIrO$_6$.

III. RESULTS AND DISCUSSION

Rietveld refined room-temperature XRD and NPD patterns of La$_2$NiIrO$_6$ are shown in Figs. 1(a) and 1(b). The refined lattice parameters are detailed in Fig. 1(a). All peaks are well indexed with the monoclinic space group $P2_1/n$, consistent with the literature [23], and there is no sign of any impurity phase.

Figures 2(a) and 2(b) display the zero-field cooled (ZFC) and field-cooled (FC) DC magnetization curves measured for La$_2$NiIrO$_6$ as a function of temperature and magnetic field. The ZFC and FC curves measured at 500 Oe are shown in Fig. 2(a) and the inset shows the ZFC curves measured by applying 100 Oe, 500 Oe, 1 kOe, and 10 kOe fields.

As the sample is cooled from room temperature, a small cusp appears at 74 K corresponding to the AFM ordering of Ni^{2+} and Ir^{4+} moments as confirmed by the neutron diffraction study discussed below. In addition to this AFM ordering, two additional anomalies are evident in the ZFC curve at 50 and 28 K, consistent with the magnetization results on single-crystal samples of La$_2$NiIrO$_6$, which show two additional magnetic transitions at roughly 30 and 60 K in the applied field of 1 kOe that are suppressed in the applied of 10 kOe, shown in Ref. [39]. A similar anomaly at low temperature (54 K) has also been observed in La$_2$CuIrO$_6$ and has been attributed to a weak ferromagnetic component [34], similar to the Ru-based double perovskites where a weak ferromagnetic component was expected [26,28]. With increasing applied field, the two transitions at 28 and 50 K smear out and only a broad peak can be seen in the ZFC curve measured at 10 kOe. The inverse susceptibility is plotted in the inset of Fig. 2(b). The Curie-Weiss fit gives the value of the effective paramagnetic moment (μ_{eff}) to be 3.38 μ_B/f.u. and the
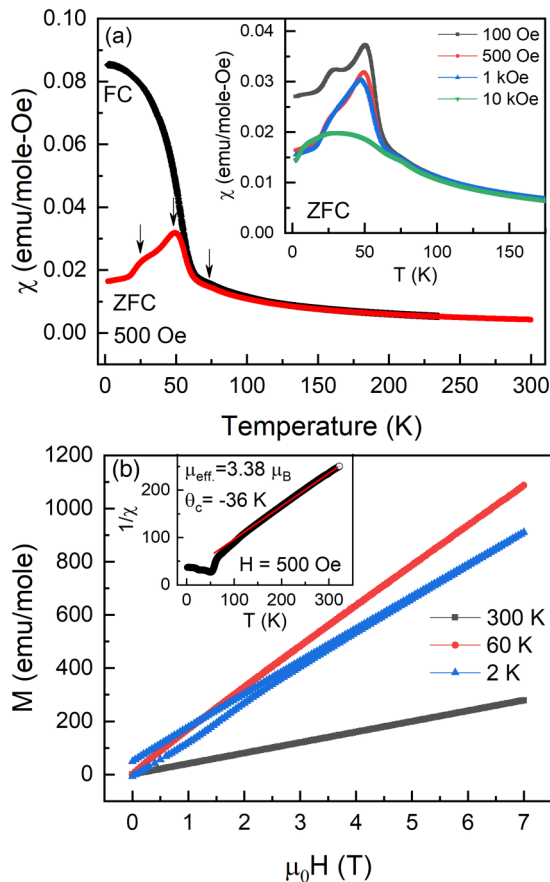
FIG. 2. (a) The ZFC and FC DC susceptibility of La_2NiIrO_6 as a function of temperature measured with 500-Oe field. The inset shows the ZFC curves measured with 100 Oe, 500 Oe, 1 kOe, and 10 kOe applied field. The arrows highlight the anomalies observed as a function of temperature. (b) Magnetization isotherms recorded at various temperatures. A clear hysteresis is observed at 2 K. The inset shows the inverse susceptibility vs temperature curve and the solid line shows the fit to Curie-Weiss behavior.

Curie-Weiss temperature θ_C to be -36 K. The value of μ_{eff} is in close agreement with the spin-only value expected for Ni^{2+} ($S = 1$, $\mu_{eff} = 2.83\,\mu_B$) and Ir^{4+} ($S = 1/2$, $\mu_{eff} = 1.73\,\mu_B$)
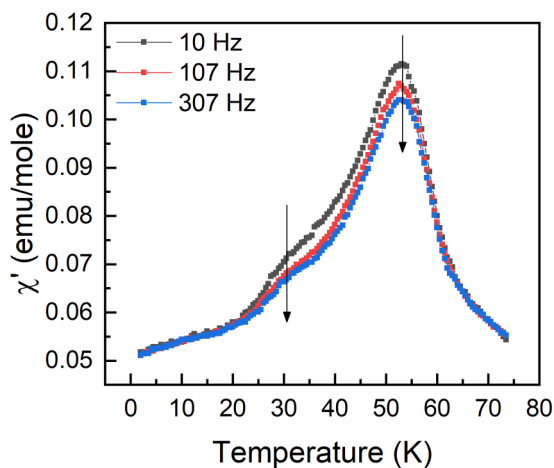

FIG. 3. The AC susceptibility of La_2NiIrO_6 measured with 10, 107, and 307 Hz.
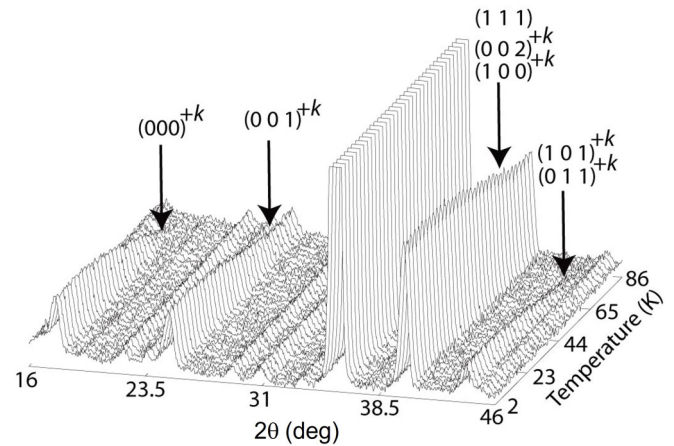

FIG. 4. Thermal neutron powder diffractogram recorded between 1.5 and 88 K showing the appearance of magnetic peaks at about 74 K.

ions which is $3.32\,\mu_B$. The isothermal magnetization curves measured at 2, 60, and 300 K are displayed in Fig. 2(b). The M vs H curves for 300 and 60 K are almost linear while a small hysteresis is observed at 2 K which indicates that a small ferromagnetic component exists at 2 K with dominating AFM interactions. This agrees with the FC susceptibility data, which reveal FM-type behavior [Fig. 2(a)].

Figure 3 exhibits the AC susceptibility behavior of La_2NiIrO_6 measured with different frequencies. The temperatures of all the anomalies are frequency independent as highlighted by the arrows in the figure. The 74 K anomaly is hard to see in the AC susceptibility data and can only be seen in an enlarged view.

High-resolution NPD from D2B at 1.5 K confirm that the monoclinic structure with symmetry $P2_1/n$ remains the same at low temperature. While the unit-cell a and c parameters have decreased at 1.5 K [$a = 5.5624(2)$ Å, $b = 5.6205(2)$ Å, $c = 7.8805(3)$ Å] the b parameter expands slightly compared to the room-temperature values. The high-intensity temperature-dependent neutron diffraction data (Fig. 4)
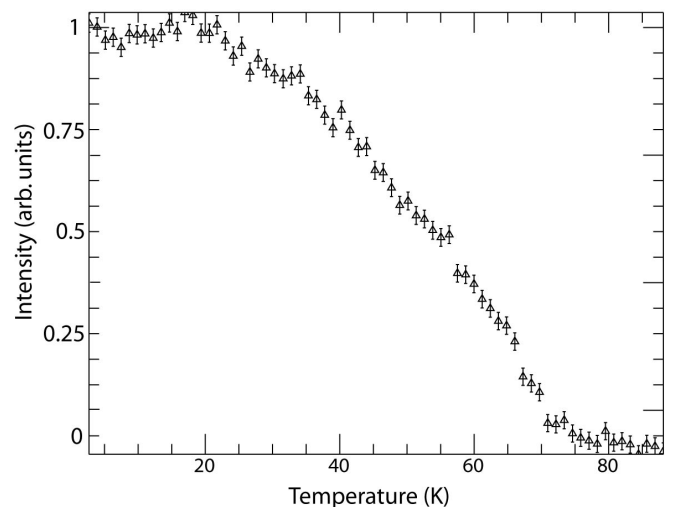

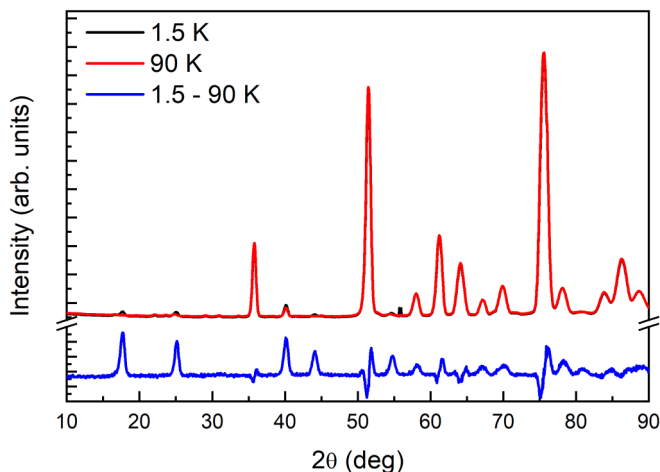FIG. 5. Temperature dependence of the $(000)^{+k}$ magnetic peak.

FIG. 6. Neutron diffraction patterns recorded at 1.5 and 90 K along with the difference curve (1.5–90 K) shown at the bottom using the blue curve. The difference curve has been magnified by a factor of 10.

reveals the appearance of new peaks (at, e.g., $2\theta = 17.55°$, $24.9°$, etc.) below about 74 K. All magnetic peaks can be indexed with the propagation vector $k = (1/2, 1/2, 0)$. It can be noted that no new peaks appear below the other two magnetic anomalies, i.e., 50 and 28 K. Furthermore, the temperature variation of the magnetic peaks does not show any change in position or intensity at these macroscopically determined anomalies.

This is further illustrated in Fig. 5, where the temperature dependence of the strongest magnetic peak (000^{+k}) is shown. The increase in intensity is continuous below 74 K down to 20 K where the intensity plateaus down to 1.5 K without showing any anomalies, as seen in the macroscopic magnetization data, at the temperatures 28 and 50 K.

This indicates that the magnetic structure does not change over the whole temperature range below $T_N = 74$ K down to 1.5 K. Figure 6 shows the NPD patterns at 1.5 and 90 K measured with increased statistics as well as the difference curve

1.5–90 K (plotted with a blue color line at the bottom) which has been strongly magnified to allow a better visualization of the new peaks appearing at low temperature.

Magnetic symmetry analysis was performed using the program MAXMAGN of the Bilbao Crystallographic server. Only one magnetic space group [2-P_s-1 (No. 2.7)] allows for the presence of magnetic moments on the cation sites. Both the Ni site on 2d (½ 0 0) and the Ir site on 2c (½ 0 ½) get split under the action of the propagation vector. Each of the two Ni and two Ir sites are allowed to have magnetic components in the three unit-cell directions corresponding to the basis vectors (BVs) (100), (010), and (001). As visible from Fig. 6 the magnetic scattering contributes only a very small part of the total diffraction intensity, and a direct refinement of the low-temperature data does not allow a sensible determination of the details of the magnetic structure. Data taken with high statistics at 90 K in the paramagnetic state have therefore been refined using the crystallographic structure and the resulting scale factor has been used for the subsequent refinement of the temperature difference data sets 1.5–90 K, 40–90 K, and 6–90 K. Due to the splitting of both cation sites (2d for Ni and 2c for Ir) there are in theory 12 independent parameters available for the refinement of the magnetic structure. The limited number of magnetic peaks does not allow a refinement which gives all these 12 parameters simultaneously with the result that the refinement diverges. Constraining the components of the two Ni sites and of the two Ir sites to be the same in absolute values stabilizes the fits. Testing the different relative orientations of the magnetic components (BVs) in (100), (010), and (001) directions within the two Ni sites and relative to the couple of Ir sites leads rapidly to several excellent refinements having identical goodness of fit values. Figure 7(a) displays one of these refinements which all return identical absolute values of the magnetic components and of the total magnetic moments. The two Ni sites see 1.5 K components of $|\mu_x| = 1.30(5) \mu_B$, $|\mu_y| = 0.22(6) \mu_B$, and $|\mu_z| = 0.43(22)\mu_B$ and a total moment of $\mu_{Ni} = 1.39 \mu_B$, while the two Ir sites have $|\mu_x| = 0.14(6)\mu_B$, $|\mu_y| = 0.32(8) \mu_B$, and $|\mu_z| = 0.14(24) \mu_B$ giving $\mu_{Ir} = 0.38 \mu_B$. The magnetic form
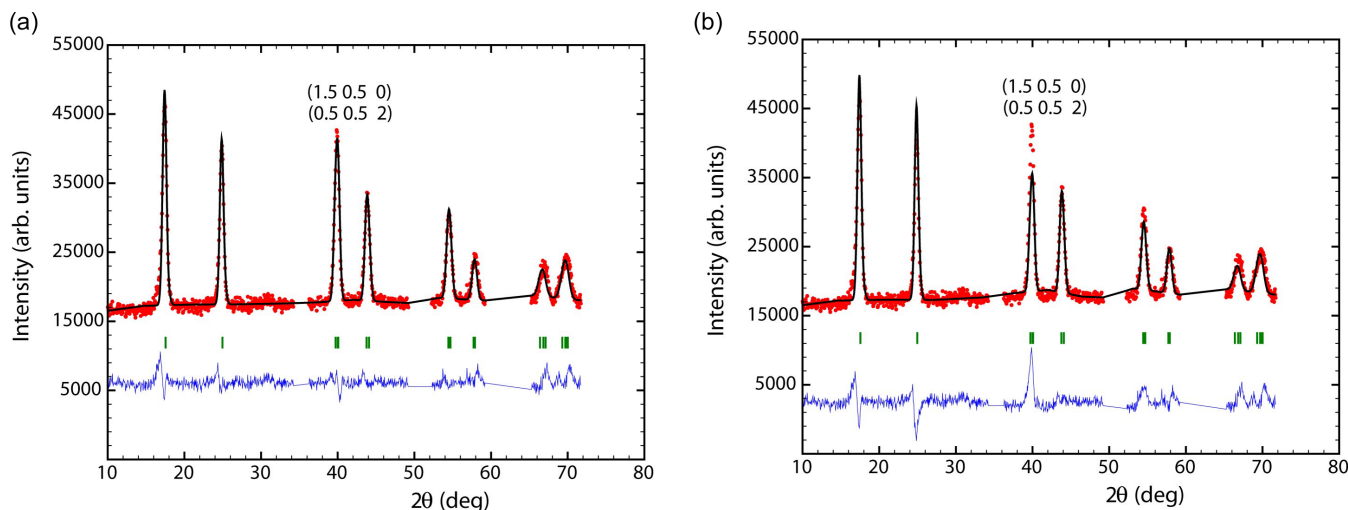
(a)

(b)

FIG. 7. (a) Rietveld refinement of the temperature difference data set 1.5–90 K with moments on both Ni and Ir sites; (b) the same assuming no magnetic moment on the Ir sites.
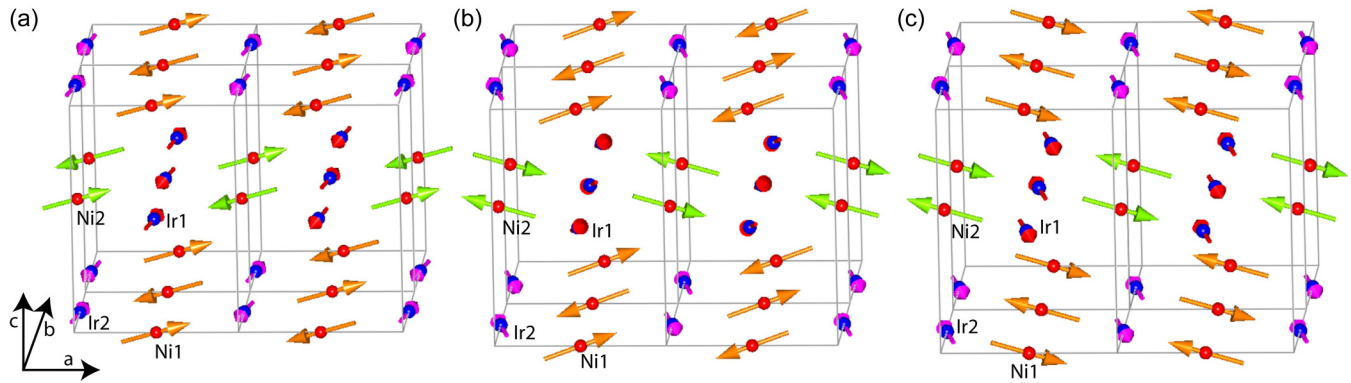
FIG. 8. Three different models of the magnetic structure which are all compatible with the refinement of the neutron data; see Table I.

factor of Ir^{4+} as published by Kobayashi *et al.* [42] has been used for the refinements.

Three of these solutions are shown in Fig. 8, and Table I lists the corresponding relative orientations of the BVs. The corresponding mcif files are provided in the Supplemental Material [43]. Neutron powder data cannot distinguish between these solutions as the magnetic reflections which change intensity dependent on the model chosen are positioned at exactly the same 2θ values as, e.g., the $(000)^{+k}$ and the $(0-10)^{+k}$ reflections which form the first magnetic peak at $2\theta = 17.5°$. Single-crystal data would be required to differentiate between the possible models. Apart from the three models shown in Fig. 8 and Table I there are three further possible solutions which are created by applying a phase shift of π on Ni2 and Ir2 or on Ni1 and Ir1. These six solutions have identical values of $R_{Mag} = 8.2$ and $\chi^2 = 6.1$. The model shown in Fig. 8(b) corresponds to the solution presented in Ref. [36] if the component in the b direction is ignored. Using our data, this solution returns notably poorer agreement: $R_{Mag} = 9.4$ and $\chi^2 = 7.6$. The presence of an ordered magnetic moment on the Ir site was not conclusively answered in Ref. [36] as the determined value of $0.17(3)\,\mu_B$ was said to be at the detection limit of the measurement and a zero moment on the Ir site could not be excluded. Figure 7(b) demonstrates that ignoring the magnetic moment on the Ir site

results in a poorer refinement of our high statistics data with differences clearly visible for several magnetic peaks and an increase in $R_{Mag} = 11.8$ and $\chi^2 = 11.7$.

The question of the simultaneous onset of magnetic order on both cation sites can be answered by looking at Fig. 9, which shows the temperature dependence of the Ni^{2+} and Ir^{4+} moments as determined using the high statistics difference datasets. The moment sizes decrease as the sample is warmed towards $T_N = 74$ K but even at 62 K, the Ir moment is $0.24(5)\,\mu_B$ and clearly measurable. The inset of Fig. 9 shows a refinement assuming the absence of an ordered magnetic moment on the Ir site. The same imperfections as seen in Fig. 7(b) can be noted and indicate strongly that both cation sites order simultaneously at T_N.

A possible ferromagnetic component as indicated by the field-cooled susceptibility data [Fig. 2(a)] and the isothermal magnetization data at 2 K [Fig. 2(b)] cannot be inferred from the NPD. This may be due to this component being induced by the application of a magnetic field or/and the sensitivity of NPD to a very small magnetic moment having $k = 0$ and giving additional magnetic intensity only on top of the nuclear peaks. The ferromagnetic moment seen in the FC susceptibility data of La_2NiIrO_6 [Fig. 2(a)] can be calculated to be approximately $7 \times 10^{-3}\,\mu_B$, a value which is significantly below the detection limit for neutron diffraction.

TABLE I. Orientations of the three basis vectors in the three models presented in Fig. 8. The refined absolute values of the BVs ($T = 1.5$ K) are identical for the three models.

	Figure 8(a)			Figure 8(b)			Figure 8(c)		
	(100)	(010)	(001)	(100)	(010)	(001)	(100)	(010)	(001)
Ni1 on ½ 0 0	+	−	+	+	+	+	+	+	−
Ni2 on 0 ½ ½	+	−	+	−	−	+	−	−	+
Ir1 on ½ 0 ½	+	+	+	+	−	+	+	−	−
Ir2 on 0 ½ 0	+	+	+	−	+	+	−	+	+

Refined absolute values of the magnetic moments

	μ_{Ni}	μ_{Ir}
(100)	1.30(5)	0.14(6)
(010)	0.22(6)	0.32(8)
(001)	0.43(22)	0.14(24)
$\mu_B{}^a$	1.39(8)	0.35(3)

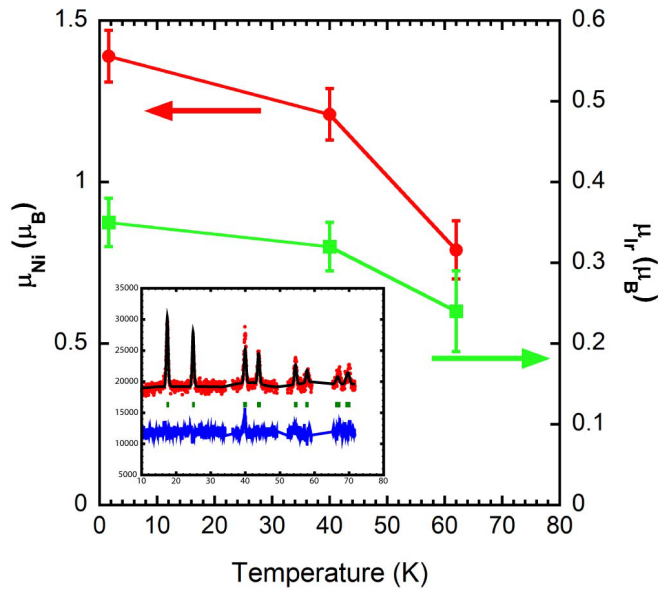^{a}Determined after setting the (001) components which have very large error bars to zero.

FIG. 9. Temperature dependence of the magnetic moment of Ni^{2+} and Ir^{4+}. As the error on the magnetic components in (001) direction is very large (see Table I for $T = 1.6$ K) this component was set to zero for the refinements.

IV. CONCLUSIONS

The magnetism of the double-perovskite La_2NiIrO_6 has been investigated using magnetization and neutron powder diffraction measurements. Temperature-dependent DC magnetization measurements reveal three anomalies at 28, 50, and 74 K, out of which only the 74 K transition is associated with the long-range ordering of Ni^{2+} and Ir^{4+} moments as confirmed from the temperature-dependent neutron diffraction study. Using very high-intensity neutron diffraction data,

additional information on the magnetic structure of La_2NiIrO_6 is presented and compared to those reported by Ferreira *et al.* [36]. Different relative orientations of the magnetic components (basis vectors) in the (100), (010), and (001) directions for the two Ni and Ir sites have been tested and shown to lead to several excellent refinements with identical goodness of fit values. All solutions return identical absolute values of the magnetic components and of the total magnetic moments. Hence, all three components (at 1.5 K) of the moment $|\mu_x| = 1.30(5)\ \mu_B$, $|\mu_y| = 0.22(6)\ \mu_B$, and $|\mu_z| = 0.43(22)\ \mu_B$ and a total moment of $\mu_{Ni} = 1.39\ \mu_B$ for the two Ni sites, and of $|\mu_x| = 0.14(6)\ \mu_B$, $|\mu_y| = 0.32(8)\ \mu_B$, and $|\mu_z| = 0.14(24)\ \mu_B$ giving $\mu_{Ir} = 0.35\ \mu_B$ for the two Ir sites can be determined unambiguously. The analysis of neutron diffraction data at various temperatures demonstrates that both the Ni and Ir moments order simultaneously at 74 K and no changes in the magnetic structure are visible in the temperature region where the magnetic data detected further anomalies. This might be related to the limits of neutron powder diffraction methods to detect very small ferromagnetic components. Further single-crystal neutron diffraction measurements and element selective resonance x-ray diffraction measurements of La_2NiIrO_6 are essential to determine the actual magnetic structure among the different solutions proposed by powder diffraction methods and to study a possible additional spin canting at low temperatures.

[1] D. I. Khomskii, *Transition Metal Compounds* (Cambridge University Press, Cambridge, 2014).

[2] A. P. Ramirez, Colossal magnetoresistance, J. Phys: Condens. Matter **9**, 8171 (1997).

[3] J. G. Bednorz and K. A. Müller, Possible high Tc superconductivity in the Ba−La−Cu−O system, Z. Phys. B: Condens. Matter **64**, 189 (1986).

[4] M. Imada, A. Fujimori, and Y. Tokura, Metal-insulator transitions, Rev. Mod. Phys. **70**, 1039 (1998).

[5] Y. Tokura and N. Nagaosa, Orbital physics in transition-metal oxides, Science **288**, 462 (2000).

[6] J. Chaloupka, G. Jackeli, and G. Khaliullin, Kitaev-Heisenberg Model on a Honeycomb Lattice: Possible Exotic Phases in Iridium Oxides A_2IrO_3, Phys. Rev. Lett. **105**, 027204 (2010).

[7] A. Shitade, H. Katsura, J. Kunes, X.-L. Qi, S.-C. Zhang, and N. Nagaosa, Quantum Spin Hall Effect in a Transition Metal Oxide Na_2IrO_3, Phys. Rev. Lett. **102**, 256403 (2009).

[8] G. Jackeli and G. Khaliullin, Mott Insulators in the Strong Spin-Orbit Coupling Limit: From Heisenberg to a Quantum Compass and Kitaev Models, Phys. Rev. Lett. **102**, 017205 (2009).

[9] D. Pesin and L. Balents, Mott physics and band topology in materials with strong spin–orbit interaction, Nat. Phys. **6**, 376 (2010).

[10] X. Wan, A. M. Turner, A. Vishwanath, and S. Y. Savrasov, Topological semimetal and Fermi-arc surface states in the electronic structure of pyrochlore iridates, Phys. Rev. B **83**, 205101 (2011).

[11] Y. K. Kim, N. H. Sung, J. D. Denlinger, and B. J. Kim, Observation of a d-wave gap in electron-doped Sr_2IrO_4, Nat. Phys. **12**, 37 (2016).

[12] Y. K. Kim, O. Krupin, J. D. Denlinger, A. Bostwick, E. Rotenberg, Q. Zhao, J. F. Mitchell, J. W. Allen, and B. J. Kim, Fermi arcs in a doped pseudospin-1/2 Heisenberg antiferromagnet, Science **345**, 187 (2014).

[13] B. J. Kim, H. Jin, S. J. Moon, J.-Y. Kim, B.-G. Park, C. S. Leem, J. Yu, T. W. Noh, C. Kim, S.-J. Oh, J.-H. Park, V. Durairaj, G. Cao, and E. Rotenberg, Novel $J = 1/2$ Mott State Induced by Relativistic Spin-Orbit Coupling in Sr_2IrO_4, Phys. Rev. Lett. **101**, 076402 (2008).

[14] F. Wilczek, Two Applications of Axion Electrodynamics, Phys. Rev. Lett. **58**, 1799 (1987).

[15] T. K. Mandal, C. Felser, M. Greenblatt, and J. Kübler, Magnetic and electronic properties of double perovskites and estimation of their Curie temperatures by ab initio calculations, Phys. Rev. B **78**, 134431 (2008).

[16] F. Wang and T. Senthil, Twisted Hubbard Model for Sr_2IrO_4: Magnetism and Possible High Temperature Superconductivity, Phys. Rev. Lett. **106**, 136402 (2011).

[17] F. Galasso and W. Darby, Preparation of single crystals of complex perovskite ferroelectric and semiconducting compounds, Inorg. Chem. **4**, 71 (1965).

[18] G. Blasse, New compounds with perovskite-like structures, J. Inorg. Nucl. Chem. **27**, 993 (1965).

[19] S. K. Pradhan, B. Dalal, R. A. Saha, R. Datta, S. Majumdar, and S. K. De, Magnetic and transport properties of the mixed 3d-5d-4f double perovskite Sm_2CoIrO_6, J. Phys.: Condens. Matter **33**, 335801 (2021).

[20] G. Cao, T. F. Qi, L. Li, J. Terzic, S. J. Yuan, L. E. DeLong, G. Murthy, and R. K. Kaul, Novel Magnetism of $Ir^{5+}(5d^4)$ Ions in the Double Perovskite Sr_2YIrO_6, Phys. Rev. Lett. **112**, 056402 (2014).

[21] A. Kolchinskaya, P. Komissinskiy, M. B. Yazdi, M. Vafaee, D. Mikhailova, N. Narayanan, H. Ehrenberg, F. Wilhelm, A. Rogalev, and L. Alff, Magnetism and spin-orbit coupling in Ir-based double perovskites $La_{2-x}Sr_xCoIrO_6$, Phys. Rev. B **85**, 224422 (2012).

[22] S. Vasala and M. Karppinen, $A_2B'B''O_6$ perovskites: A review, Prog. Solid State Chem. **43**, 1 (2015).

[23] M. A. Laguna-Marco, P. Kayser, J. A. Alonso, M. J. Martínez-Lope, M. van Veenendaal, Y. Choi, and D. Haskel, Electronic structure, local magnetism, and spin-orbit effects of Ir(IV)-, Ir(V)-, and Ir(VI)-based compounds, Phys. Rev. B **91**, 214433 (2015).

[24] D.-Y. Jung, G. Demazeau, and J.-H. Choy, Iridium(III) stabilized in oxygen lattices with the perovskite structure $Sr_2MIrO_6(M = Nb, Ta)$, J. Mater. Chem. **5**, 517 (1995).

[25] P. Yadav, S. Sharma, P. J. Baker, P. K. Biswas, I. da Silva, R. Raghunathan, U. Deshpande, R. J. Choudhary, N. P. Lalla, and A. Banerjee, μSR and neutron diffraction studies on the tuning of spin-glass phases in the partially ordered double perovskites $SrMn_{1-x}W_xO_3$, Phys. Rev. B **99**, 214421 (2019).

[26] D. T. Adroja, S. Sharma, C. Ritter, A. D. Hillier, D. Le, C. V. Tomy, R. Singh, R. I. Smith, M. Koza, A. Sundaresan, and S. Langridge, Muon spin rotation and neutron scattering investigations of the B-site ordered double perovskite Sr_2DyRuO_6, Phys. Rev. B **101**, 094413 (2020).

[27] S. Sharma, P. Yanda, P. Yadav, I. da Silva, and A. Sundaresan, Suppression of long-range ordering and multiferroicity in Sr-substituted $Ba_{3-x}Sr_xMnNb_2O_9$ ($x = 1$ and 3), J. Magn. Magn. Mater. **512**, 166990 (2020).

[28] S. Sharma, D. T. Adroja, C. Ritter, D. Khalyavin, P. Manuel, G. B. G. Stenning, A. Sundaresan, A. D. Hillier, P. P. Deen, D. I. Khomskii, and S. Langridge, Magnetic ground state of the ordered double-perovskite Sr_2YbRuO_6: Two magnetic transitions, Phys. Rev. B **102**, 134412 (2020).

[29] A. V. Powell, J. G. Gore, and P. D. Battle, The magnetic properties of iridium in mixed-metal oxides, J. Alloys Compd. **201**, 73 (1993).

[30] G. Cao, A. Subedi, S. Calder, J.-Q. Yan, J. Yi, Z. Gai, L. Poudel, D. J. Singh, M. D. Lumsden, A. D. Christianson, B. C. Sales, and D. Mandrus, Magnetism and electronic structure of La_2ZnIrO_6 and La_2MgIrO_6: Candidate $J_{eff} = 1/2$ Mott insulators, Phys. Rev. B **87**, 155136 (2013).

[31] S. Lee, M.-C. Lee, Y. Ishikawa, P. Miao, S. Torii, C. J. Won, K. D. Lee, N. Hur, D.-Y. Cho, and T. Kamiyama, Magnetoelastic octahedral breathing mode in the ferrimagnetic La_2CoIrO_6 double perovskite, Phys. Rev. B **98**, 104409 (2018).

[32] H.-R. Fuh, K.-C. Weng, Y.-P. Liu, and Y.-K. Wang, New ferromagnetic semiconductor double perovskites: La_2FeMO_6 (M = Co, Rh, and Ir), J. Alloys Compd. **622**, 657 (2015).

[33] A. Grimaud, A. Demortière, M. Saubanère, W. Dachraoui, M. Duchamp, M.-L. Doublet, and J.-M. Tarascon, Activation of surface oxygen sites on an iridium-based model catalyst for the oxygen evolution reaction, Nat. Energy **2**, 16189 (2016).

[34] K. Manna, R. Sarkar, S. Fuchs, Y. A. Onykiienko, A. K. Bera, G. A. Cansever, S. Kamusella, A. Maljuk, C. G. F. Blum, L. T. Corredor, A. U. B. Wolter, S. M. Yusuf, M. Frontzek, L. Keller, M. Iakovleva, E. Vavilova, H.-J. Grafe, V. Kataev, H.-H. Klauss, D. S. Inosov, S. Wurmehl, and B. Büchner, Non-collinear antiferromagnetism of coupled spins and pseudospins in the double perovskite La_2CuIrO_6, Phys. Rev. B **94**, 144437 (2016).

[35] H. E. Karaca, I. Karaman, B. Basaran, Y. Ren, Y. I. Chumlyakov, and H. J. Maier, Magnetic field-induced phase transformation in NiMnCoIn magnetic shape-memory alloys— a new actuation mechanism with large work output, Adv. Funct. Mater. **19**, 983 (2009).

[36] T. Ferreira, S. Calder, D. S. Parker, M. H. Upton, A. S. Sefat, and H.-C. zur Loye, Relationship between A-site cation and magnetic structure in 3d-5d-4f double perovskite iridates Ln_2NiIrO_6 (Ln = La, Pr, Nd), Phys. Rev. Mater. **5**, 064408 (2021).

[37] P. A. McClarty, A. D. Hiller, D. T. Adroja, D. D. Khalyavin, R. Sudhindra, M. Pascal, K. Winfried, and E. V. Sampathkumaran, Non-collinear order and spin–orbit coupling in Sr_3ZnIrO_6, J. Phys. Soc. Jpn. **89**, 64703 (2020).

[38] H. Guo, C. Ritter, and A. C. Komarek, Direct determination of the spin structure of $Nd_2Ir_2O_7$ by means of neutron diffraction, Phys. Rev. B **94**, 161102(R) (2016).

[39] T. Ferreira, G. Morrison, J. Yeon, and H.-C. zur Loye, Design and crystal growth of magnetic double perovskite iridates: Ln_2MIrO_6 (Ln = La, Pr, Nd, Sm-Gd; M = Mg, Ni), Cryst. Growth Des. **16**, 2795 (2016).

[40] J. Rodríguez-Carvajal, Recent advances in magnetic structure determination by neutron powder diffraction, Phys. B: Condens. Matter **192**, 55 (1993).

[41] M. I. Aroyo, J. M. Perez-Mato, C. Capillas, E. Kroumova, S. Ivantchev, G. Madariaga, A. Kirov, and H. Wondratschek, Bilbao Crystallographic Server: I. Databases and crystallographic computing programs,, Z. Kristallogr.: Cryst. Mater. **221**, 15 (2006).

[42] K. Kobayashi, T. Nagao, and M. Ito, Radial integrals for the magnetic form factor of 5d transition elements, Acta Crystallogr. A **67**, 473 (2011).

[43] See Supplemental Material at http://link.aps.org/supplemental/10.1103/PhysRevMaterials.6.014407 for mcif files for magnetic structure analysis of La_2NiIrO_6.

[44] DOI: 10.5291/ILL-DATA.5-31-2675.